Observation of the scalar Aharonov-Bohm effect by neutron interferometry

B. E. Allman, A. Cimmino, A. G. Klein, and G. I. Opat
School of Physics, University of Melbourne, Parkville, Victoria 3052, Australia

H. Kaiser and S. A. Werner
Department of Physics and Research Reactor Center, University of Missouri–Columbia, Columbia, Missouri 65211
(Received 12 March 1993)

A phase shift for de Broglie waves due to the action of a scalar potential in an otherwise field-free (i.e., force-free) region of space is known as the scalar Aharonov-Bohm (AB) effect. Unlike the more familiar AB effect due to the magnetic vector potential, the scalar effect has hitherto remained unverified due, presumably, to technical difficulties in electron interferometry. We have performed an analogous interferometric experiment with thermal neutrons subject to pulsed magnetic fields. The observations were carried out at the University of Missouri Research Reactor using a skew-symmetric perfect-silicon-crystal neutron interferometer. The expected phase shifts have been observed to a high degree of accuracy. A detailed description of the experiment and its interpretation is given in this paper.

PACS number(s): 03.65.Bz, 42.50.−p

I. HISTORICAL INTRODUCTION

According to classical Maxwell theory of electrodynamics, potentials are merely a convenient mathematical tool for calculating the electromagnetic fields of force. However, in quantum mechanics potentials have a primary physical significance and are an essential ingredient which cannot be readily eliminated from the Schrödinger equation. In the historic paper entitled "Significance of Electromagnetic Potentials in Quantum Theory" published in 1959, Aharonov and Bohm [1] proposed two types of actual electron interference experiments aimed at exhibiting these conclusions. The phenomena predicted came to be known as the Aharonov-Bohm (AB) effect, and have given rise to a substantial literature over the past 30 years.

The essential physical aspect of the AB experiments [2] is that electrons suffer phase shifts in passing through regions of space of zero fields but nonzero potentials. The effects are of two types, the magnetic (or vector) AB effect, and the electric (or scalar) AB effect, now discussed in turn.

A. Magnetic AB effect

In Fig. 1(a), the de Broglie wave of an electron is shown as coherently split into two parts, which jointly encircle a region of space containing a tube of magnetic flux. The electron paths are entirely in field-free (and hence force-free) regions of space. However, the magnetic vector potential $\mathbf{A}$, which cannot be zero along all of both of these paths, give rise to a phase shift $\Delta\phi_{\mathrm{AB}}$, between the two halves of the wave, namely,

$$\Delta\phi_{\mathrm{AB}}=(1/\hbar)\oint \mathbf{p}\cdot\mathbf{dx} =(e/\hbar c)\oint \mathbf{A}\cdot\mathbf{dx} , \quad (1)$$

where the canonical momentum $\mathbf{p}$ is given by

$$\mathbf{p}=(m\mathbf{v}+e\,\mathbf{A}/c) . \quad (2)$$

Using Stokes's theorem and the magnetic field, $\mathbf{B}=\nabla\times\mathbf{A}$, the phase shift $\Delta\phi_{\mathrm{AB}}$ is seen to be proportional to the magnetic flux, Φ_M, enclosed by the paths

$$\Delta\phi_{\mathrm{AB}}=(e/\hbar c)\int \mathbf{B}\cdot\mathbf{ds}=(e/\hbar c)\Phi_M . \quad (3)$$

The observation of just such a phase shift was the subject of several experiments, first by Chambers [3] in 1960, who used crystalline whiskers of iron as tubes of flux inside an electron microscope adapted to function as an electron interferometer. Möllenstedt and Bayh [4], in 1962, used micrometer-sized current-carrying solenoids inside their electron interferometer. More recently, definitive experiments in electron holography, carried out by Tonomura *et al.* [5], employed tiny ferromagnetic toroids, made of thin films of permalloy. In all these cases the predicted effects were indeed observed.

Nevertheless, extensive controversy has accompanied the AB effect, in spite of the important paper by Furry and Ramsey [6] which back in 1960 pointed out that the AB effect is essential for the self-consistency of quantum mechanics. They showed that the effect is of just the right magnitude to destroy the interference pattern if one

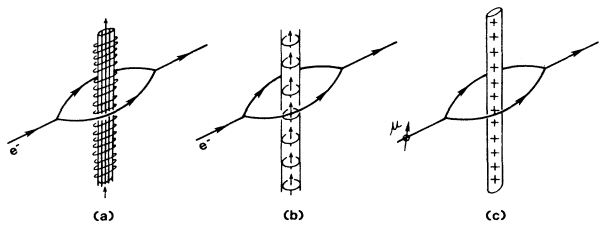

FIG. 1. Schematic diagram of (a) the magnetic Aharonov-Bohm experiment, (b) equivalent Aharonov-Bohm experiment, (c) the duality between the AB and Aharonov-Casher topology.

were to attempt to determine which of the two paths the particle has taken around the tube of flux. The interpretation of the various experiments also gave rise to extensive discussion and commentary because of the fundamental nature of the conclusions reached. The high precision of Tonomura's experiments leaves little room for quibble, but alternative theoretical ideas have appeared from time to time. For a detailed summary of these discussions refer to the excellent review by Olariu and Popescu [7]. For our purposes, it is interesting to note that similar discussion was engendered by some of the neutron experiments which concern us here.

B. Electric AB effect

The electric, or scalar, AB effect for charged particles is conceptually quite simple. It concerns the phase shift caused by the scalar potential $V=-eU$ in the Schrödinger equation:

$$(H_0+V)\Psi=\frac{i\hbar\partial\Psi}{\partial t} . \tag{4}$$

Figure 2(a) shows a divided electron wave packet traveling down two conducting cylinders which act as Faraday cages, i.e., have a field-free interior irrespective of their electrostatic potentials, U_1 and U_2. To exhibit the scalar AB effect, the potential of cylinder 2 alone is pulsed while the wave packet is enclosed. In spite of the absence of force at all times, a relative phase shift, $\Delta\phi$, is predicted,

$$\Delta\phi=(e/\hbar)\int[U_2(t)]dt . \tag{5}$$

The correctness of this AB prediction is of such importance to the consistency of quantum mechanics that the actual experiment deserves a serious attempt. However, the experiment has not yet been performed because of technical difficulties with electron interferometers. The closely related experiment of Mateucci and Pozzi [8] which involves forces acting on the electron is not, therefore, a clear-cut test of the effect. Realizations with protons or ions are hindered by the lack of suitable interferometers for such particles.

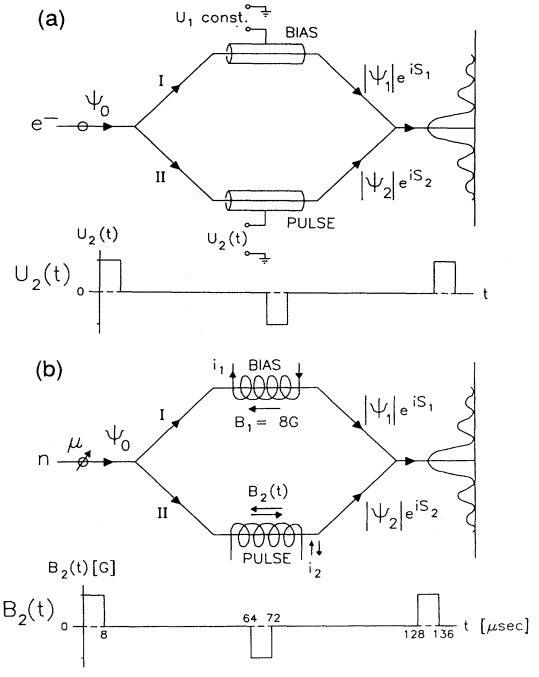

FIG. 2. Schematic diagram of (a) the scalar Aharonov-Bohm experiment for electrons and (b) the scalar Aharonov-Bohm experiment with neutrons. The wave forms of the applied pulses are also shown.

C. Search for the Aharonov-Bohm effect with neutrons

From the standard minimal electromagnetic coupling scheme one would not expect a magnetic AB effect for neutrons because of their electrical neutrality, in fact [9] $q_n<(-0.4\pm1.1)\times10^{-21}e$. Greenberger *et al.* [10] postulated an additional coupling of the form

$$V=\gamma(e/mc)\,\mathbf{A}\cdot\mathbf{p}f[(p/mc)^2] , \tag{6}$$

which they sought experimentally. In Eq. (6), γ is to be determined experimentally, and the form factor f obeys $f(0)=1$. Their experiment involved a perfect-crystal neutron interferometer in a topology similar to that of Fig. 1(a). Upon reversal of the enclosed magnetic flux of some 152 G cm^2, carried by a rectangular loop of iron, a phase shift of less than $0.56°\pm0.67°$ resulted. In consequence, they found $\gamma<4.9\times10^{-12}$; i.e., there is no AB effect of this type for neutrons.

D. The Aharonov-Casher effect

In 1984 Aharonov and Casher [11] (AC) put forward another topological effect closely related to the AB effect, in which a phase shift arises when a neutral magnetic-dipole-bearing particle diffracts around a line of electric charge. In the AC effect, just as in the AB effect, there is no force acting on the particles. In the AB effect a charge diffracts around an electrically neutral tube of magnetic flux [Fig. 1(a)], i.e., a current-carrying solenoid, or equivalently a line of dipoles [Fig. 1(b)]. In the AC effect, its dual [12], a dipole diffracts around a line charge. An alternative view [13] is that the AC effect is a consequence of the term $(\boldsymbol{\mu}/c\times\mathbf{E})$ in the canonical momentum, $\mathbf{p}=(m\mathbf{v}+\boldsymbol{\mu}/c\times\mathbf{E})$, of a neutral particle of magnetic moment $\boldsymbol{\mu}$ in an electric field $\mathbf{E}$. The AC phase shift is given by

$$\Delta\phi_{\mathrm{AC}}=(1/\hbar c)\oint\boldsymbol{\mu}\times\mathbf{E}\cdot\mathbf{ds} . \tag{7}$$

By Gauss's law Eq. (7) becomes

$$\Delta\phi_{\mathrm{AC}}=\sigma\frac{4\pi\mu\Lambda}{\hbar c} , \tag{8}$$

where Λ is the charge line density encircled by the particle; $\sigma=+1$ for spin-up particles and $\sigma=-1$ for spin-down particles with respect to the z axis, defined to be along the line charge. The AC prediction has been

verified by Cimmino *et al.* [14] (see also Kaiser *et al.* [15] and Goldhaber [16]) for a thermal neutron of magnetic moment, μ diffracting around a charged electrode, using a neutron interferometer containing a 30-kV/mm vacuum electrode system. As pointed out by Aharonov and Casher, their phase shift depends upon the linear charge density (along the axis perpendicular to the plane of the interferometer) enclosed by the beam paths, but not on any details of the geometry of the beam paths relative to the line charge. In this sense the AC effect is topological. Consequently, instead of a single line charge, a prism-shaped electrode system was used. In the geometry and conditions of the experiment, the theoretically predicted phase shift was only 1.52 mrad. The phase shift observed was 2.11 ± 0.34 mrad.

II. THE SCALAR AHARONOV-BOHM EXPERIMENT WITH NEUTRONS

The basic idea of the present experiment with neutrons was first put forward by Zeilinger [17] and later by Anandan [18,19] who pointed out that one can obtain a phase shift due to a scalar potential, $V=-\boldsymbol{\mu}\cdot\mathbf{B}$, as the analog of $V=-eU$, the scalar potential in the "electric" scalar AB effect for electrons. This parallels the previous situation in the Aharanov-Casher experiment with neutrons which was the analog of the vector AB effect for electrons [13,18,19]. Consider a split neutron wave packet entering the solenoids in Fig. 2(b). A current pulse $i_2(t)$ is applied while the neutron is in the force-free interior of solenoid 2. The resulting magnetic field $B_2(t)$ gives rise to a phase shift.

$$\Delta\phi=(\sigma/\hbar)\int\mu B_2(t)dt\ , \tag{9}$$

analogous to Eq. (5). In Eq. (9) $\sigma=\pm1$ depending on whether the neutron is spin up or down relative to the magnetic field, the direction of quantization. In the actual experiment, short-duration current pulses, chosen to be 8 μs wide, were applied to a suitably designed solenoid placed inside a single-crystal neutron interferometer.

The purpose of this paper is to review, in some detail, our neutron-interferometric observation of the scalar AB phase shift. A brief account of the results of this experiment has already been reported [20]. Conceptually the most direct demonstration of the scalar AB effect with neutrons, as pointed out by Peshkin, would be to use neutrons polarized so their spin was in the same direction as the applied magnetic field [21]. However, our experiment was carried out with an unpolarized beam of neutrons, which can be viewed as an incoherent mixture of $\sigma=+1$ and $\sigma=-1$ neutrons. To observe the AB spin-dependent phase shift with unpolarized neutrons requires that the spin-independent phase shift in the interferometer be judiciously adjusted, as we will discuss in detail in Sec. II B below.

The experiment, shown schematically in Fig. 3 was carried out at the University of Missouri Research Reactor (MURR), using a collimated, monochromatic neutron beam ($\lambda=2.35$ Å) incident upon a monolithic, skew-symmetric, perfect-silicon-crystal neutron interferometer [22]. In such a device (see inset in Fig. 3), Bragg

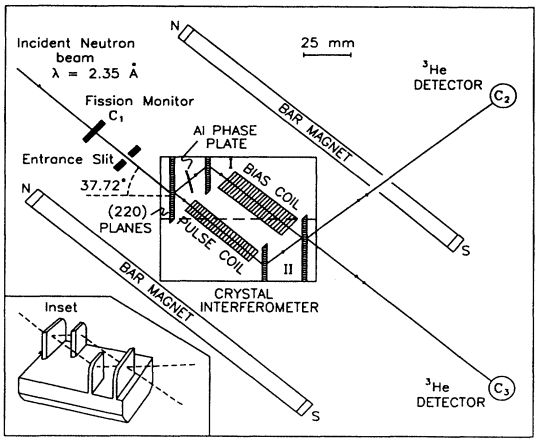

FIG. 3. Layout of the neutron scalar AB experiment using a skew-symmetric single-Si-crystal neutron interferometer. Inset: An isometric view of the interferometer crystal.

diffraction by the (220) planes at the first crystal plate divides the incident de Broglie wave front into two coherent beams. Each of these is deflected by diffraction at the intermediate crystal plates and after traversing the two solenoids (marked "pulse coil" and "bias coil"), the two beams recombine at the last crystal plate. The whole arrangement is akin to the Mach-Zehnder interferometer of classical optics [23].

A. Experimental setup

The experiment was carried out at beam port C at MURR. A schematic diagram of this beam station is shown in Fig. 4. A thermal neutron beam is channeled out of the reactor through the beam port and onto a vertically focusing two-crystal pyrolytic graphite (002) monochromator. The Bragg angle ($\theta_B=20.5°$), being fixed by the exit tube, yields a nominally monochromatic beam with $\lambda=2.349$ Å ($\Delta\lambda/\lambda\sim0.012$). The beam is filtered by a 5-cm-thick block of pyrolytic graphite to remove second-order ($\lambda/2$) neutrons and is then incident upon the interferometer. The interferometer, a single-silicon crystal, is of four-blade skew-symmetric design. The advantage with this geometry is that the beams run parallel over a good part of the interferometer. This interferometer has already been used and described in several papers [22].

The interferometer (resting in a cradle) and ^{3}He proportional detectors are housed in a small aluminum box ($40\times40\times40$ cm^3), which provides an isothermal enclosure. This box is mounted rigidly in a 5-cm-thick, 1.2×1.8 m^2 masonite box. The masonite box, with Plexiglas top, sits on an 850-kg granite slab, which in turn rests on four Firestone pneumatic vibration isolators, mounted on steel posts imbedded in a sand enclosure. Hanging below the granite slab, attached to the masonite box, is a large aluminum plate which supports 710 kg of lead bricks, used to lower the center of gravity. This entire apparatus is enclosed in an even larger Plexiglas structure to provide additional isolation against tempera-

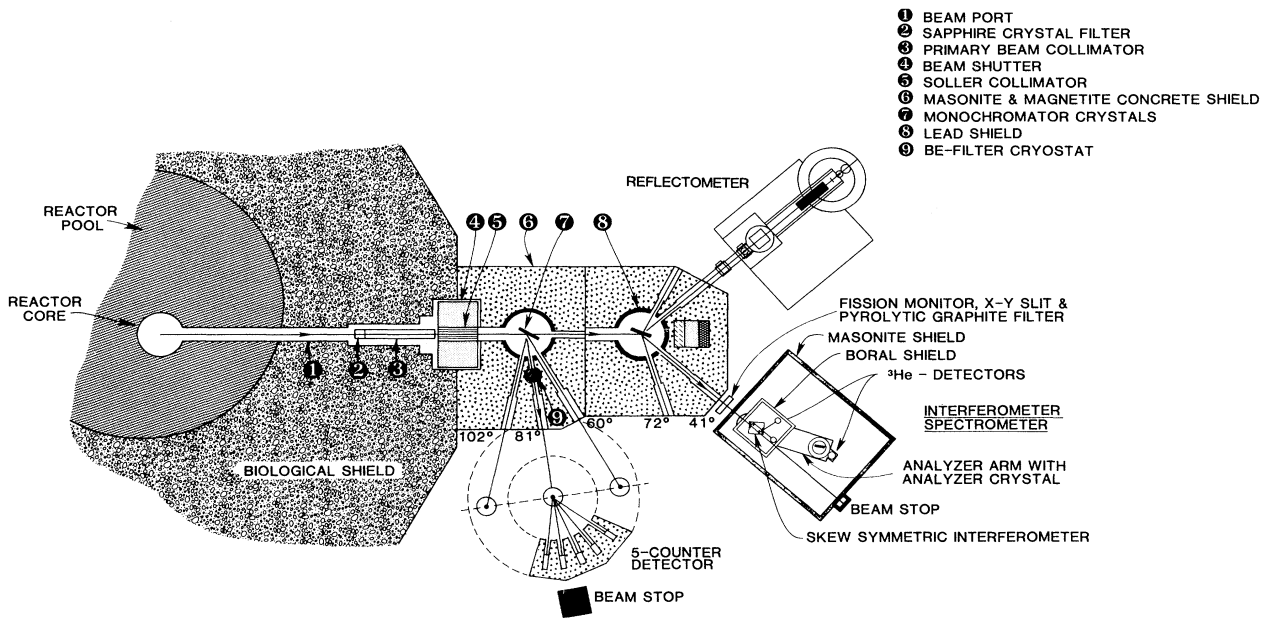

FIG. 4. Schematic of the overall *C*-port interferometer apparatus, including the reactor, beam port, shielding, and interferometer setup.

ture gradients and microphonics produced by air currents.

Two slits are used to define the neutron beam. A large one, at the masonite box, merely reduces the background, while the entrance slit, mounted on the aluminum box (10 cm from the interferometer), defines the size and location of the beam incident upon the interferometer. For the typical arrangement of a 3×4 mm^2 entrance slit the monochromatic beam intensity is of order 2×10^5 neutrons/min.

As mentioned earlier, neutrons used in this experiment were not polarized, but it was necessary to align the direction of quantization along the solenoid axes. This was achieved by means of a background magnetic field, designed to be rather uniform over the neutron path within the interferometer crystal, a volume of some $100\times30\times15$ mm^3. Owing to size limitations and possible problems with Joule-heating effects, instead of Helmholtz coils we used four permanent magnets mounted symmetrically around the interferometer. Each consisted of a soft iron bar with Nd-Fe-B permanent-magnet caps at each end. This arrangement achieved fields of between 5 and 8 G along the quantization axis, with at most a few percent transverse component at the extremities of the beam paths in the interferometer.

An important feature of the experimental design was to achieve a very uniform pulsed magnetic field over as great a length as possible between the interferometer blades. This was achieved using 45-mm-long solenoids of ~170 turns wound in a tightly packed single layer on hollow formers. These were supplemented at each end by a pair of computer designed trim coils, of opposing polarity. This configuration yielded a field of measured uniformity better than 1% over ~30-mm span on axis, which decreased rapidly to zero outside the coil. At the de Broglie wavelength employed, the neutron speed was 1.68 mm/μs, yielding more than 17 μs of flight time in the uniform region. This is just over twice the 8-μs-wide current pulses (rise time <1 μs) which corresponded to 13.5 mm of neutron travel distance. According to Eq. (9), a field of 21 G results in a phase shift $\Delta\phi_{AB}=\pi/2$ rad. The field profile of the two coils was measured with a search coil; the results are shown in Fig. 9(a).

The coils, held in aluminum blocks in a locating frame, were positioned to enclose the neutron beams. A photograph of the coil assembly, together with the soft iron bars and magnets providing the background field mounted on the same structure is shown in Fig. 5. Note the "pulse coil" housing is slotted to minimize eddy currents, whose presence initially reduces the applied field.

B. Experimental strategy

Since the phase shift produced by the magnetic fields in the solenoids depends on the relative orientation of the neutron spin, it may appear that the use of polarized neutrons is mandatory. However, by applying a well-defined adjustable bias field in the second solenoid, one gains separate control over the phase shift for the spin-up and spin-down states thus allowing the AB phase to be measured simultaneously for both, as described below. The neutron-counting rates in the recombined beams, detected by the ^{3}He counters C_2 and C_3 are given by

$$N_2=N_1(a_2-b_2\cos\Delta\phi) \tag{10a}$$

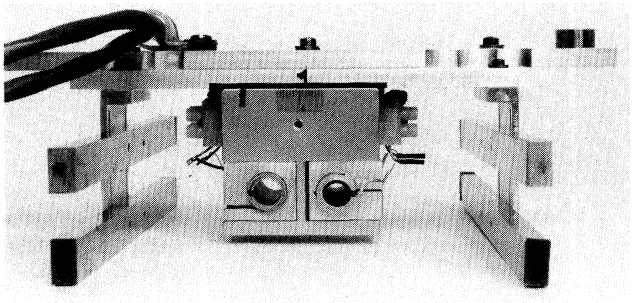

FIG. 5. Photograph of the coil assembly positioned so as to encompass the two arms of the interferometer. The smaller solenoid (right) is the pulsed coil. The quadrupole of bar magnets providing the environment field that establishes the direction for quantization for the neutron spins are seen to the sides.

and

$$N_3 = N_1(a_3 + b_3 \cos\Delta\phi) , \tag{10b}$$

where $\Delta\phi$ is the phase shift along path II relative to path I and N_1 is the counting rate in the monitor counter C_1. The constants a_2, a_3, b_2, and b_3, such that $a_2/a_3 \approx 2.5$ and $b_2 \approx b_3$, characterize the interferometer. It is found that $N_2 + N_3$ is independent of $\Delta\phi$, i.e., as $\Delta\phi$ is varied the neutrons are swapped back and forth between C_2 and C_3 (as expected by particle conservation) showing that b_2 and b_3 are equal.

As is common practice, a thin aluminum plate inserted in beam I allowed the phase of the spin-up and spin-down states to be shifted by equal amounts, $\Delta\phi_{\rm Al}$. However, the magnetic field in the bias coil shifts the phase of the spin-up and spin-down states by equal but opposite amounts, $\Delta\phi_m$. Thus, by adjusting both the orientation of the Al phase plate and the dc current in the bias coil, it is possible to control separately the phase shifts for the spin-up and spin-down states. With these appropriate phases, it is possible to determine the AB phase shift $\Delta\phi_{\rm AB}$ (produced in the pulse coil) with maximum sensitivity even using unpolarized beams. This may be seen by writing the total phase as

$$\Delta\phi = \Delta\phi_0 - \Delta\phi_{\rm Al} + \sigma(\Delta\phi_{\rm AB} - \Delta\phi_m) , \tag{11}$$

where $\Delta\phi_0$ is the offset phase of the interferometer and $\sigma = \pm 1$ for spin up or down.

The count rate in detector C_3 for spin up neutrons is

$$N_3^{\uparrow} = \tfrac{1}{2} N_1 \{ a_3 + b_3 \cos[\Delta\phi_0 - \Delta\phi_{\rm Al} + (\Delta\phi_{\rm AB} - \Delta\phi_m)] \} , \tag{12}$$

while for spin-down neutrons we have

$$N_3^{\downarrow} = \tfrac{1}{2} N_1 \{ a_3 + b_3 \cos[\Delta\phi_0 - \Delta\phi_{\rm Al} - (\Delta\phi_{\rm AB} - \Delta\phi_m)] \} . \tag{13}$$

Thus for an unpolarized incident neutron beam, N_3 is given by

$$N_3 = N_1 \{ a_3 + b_3 \cos[\Delta\phi_0 - \Delta\phi_{\rm Al}] \cos[\Delta\phi_{\rm AB} - \Delta\phi_m] \} . \tag{14a}$$

Similarly,

$$N_2 = N_1 \{ a_2 - b_2 \cos[\Delta\phi_0 - \Delta\phi_{\rm Al}] \cos[\Delta\phi_{\rm AB} - \Delta\phi_m] \} . \tag{14b}$$

Rotating the aluminum plate so that $\Delta\phi_0 - \Delta\phi_{\rm Al} = 0 (\mathrm{mod} 2\pi)$ and setting the current in the bias coil so that $\Delta\phi_m = (n + \frac{1}{2})\pi$, we establish a situation such that

$$N_3 = N_1 [a_3 + (-1)^n b_3 \sin\Delta\phi_{\rm AB}] \tag{15a}$$

and

$$N_2 = N_1 [a_2 - (-1)^n b_2 \sin\Delta\phi_{\rm AB}] . \tag{15b}$$

The obvious question that arises is: How does one know when to apply the pulses so as to catch the neutrons just as they traverse the center of the solenoid? The equally obvious answer is to apply the pulses cyclically and to gate each detected neutron into a separate scalar according to its arrival time within the cycle. In this way the phase shift of neutrons which traversed the solenoids when the current was zero can be compared with the phase shift of neutrons which traversed the center of the solenoids when the current, and hence the magnetic field, was nonzero.

The detected neutron counts were gated cyclically into a multichannel scalar with 64 channels, each of 2-μs width. This was synchronized to the 128-μs period of the current pulses applied to the solenoid. Detectors C_2 and C_3 were accurately positioned to be equidistant from the interferometer exit. Thus, within every cycle, the position of the neutrons at the time of the pulse may be deduced from the known neutron velocity and the time of detection. The finite diameter of the neutron detectors leads to a position uncertainty which corresponds to a time uncertainty of $\approx \pm 1.75$ μs, short compared with the pulse duration and the transit time through the region of uniform field.

Finally, runs were made with increasing values of the current in the pulse coil, corresponding to fields from 0 to about 30 G ($\Delta\phi_{\rm AB} = 0$ to about $3\pi/4$) in the forward as well as in the reverse direction.

C. Experimental results

The following experimental procedure was used: (i) With zero bias and pulse fields, $\Delta\phi_{\rm Al}$ was scanned by rotating the aluminum plate. (ii) The bias field was then adjusted until the amplitude of an interferogram scan was reduced to zero, thereby setting $\Delta\phi_m = (n + \frac{1}{2})\pi$. In fact, the lowest current to achieve this was used, as this minimized the Joule heating which became significant at $\Delta\phi_m \approx 3\pi/4$, thus diminishing the interference contrast. (iii) With the bias field again set to zero, another $\Delta\phi_{\rm Al}$ scan maximized N_3, so that $\Delta\phi - \Delta\phi_{\rm Al} = 0 (\mathrm{mod} 2\pi)$. (iv) The bias field was then returned to the value previously found in (ii). In the actual experiment, the magnetic phase was found to be extremely stable but the spin-

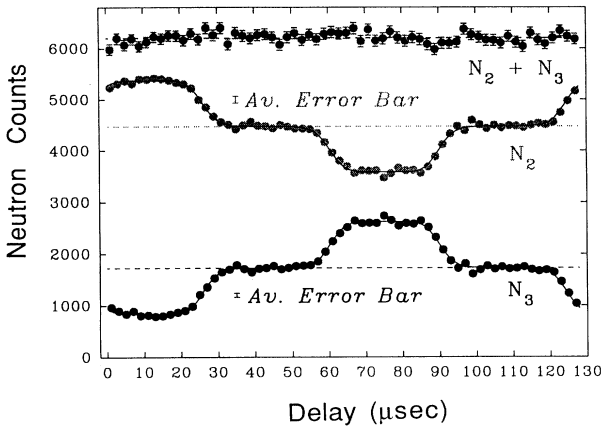

FIG. 6. Scan of counts per channel in the two detectors N_2, N_3, and their sum, plotted against delay time, for the particular case of pulsed field amplitudes of ± 19 G, which corresponds to $\Delta\phi_{AB}=1.4$ rad. The solid lines are theoretical fits, as described in the text. The total data collection time for this scan was about 10 h.

independent phase drifted by up to 150 mrad per week and so required reoptimization every few days.

The experimental runs, each lasting about 10 h, consisted of 6×10^8 full cycles of 128 μs. Each cycle contained a positive and a negative 8-μs-wide current pulse, 64 μs apart [Fig. 2(b)]. The results of such a run in the form of normalized counts in each time-delay channel for

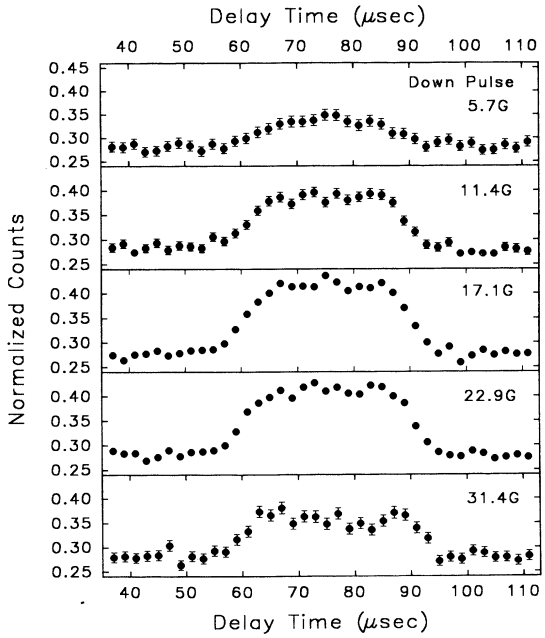

FIG. 7. Scans of the gated neutron counts for the "down" (opposite to beam direction) pulse in the cycle, for the range of applied magnetic fields. The $\pi/2$ phase shift occurs for a field of ~ 21 G. Note the loss in intensity, most noticeable for the high-field (i.e., high-current) scan, due to the Joule-heating effect in the coil reducing contrast.

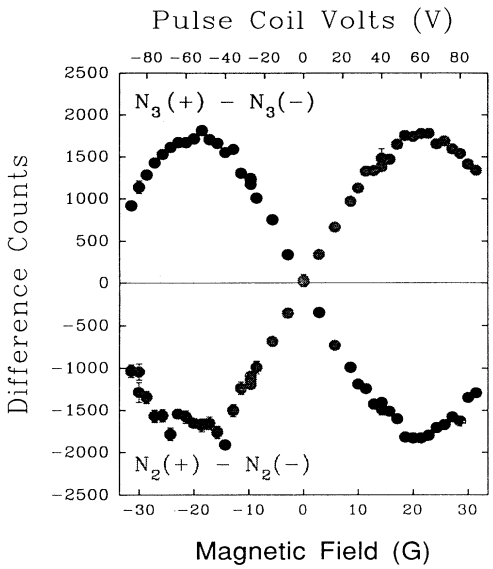

FIG. 8. Interferometer output signals as a function of pulse coil field strengths. This is obtained from the average of the central four points in each plateau region of data sets such as the one shown in Fig. 6. (Certain kinds of systematic error are avoided by taking the difference between the counts for positive and negative pulses.)

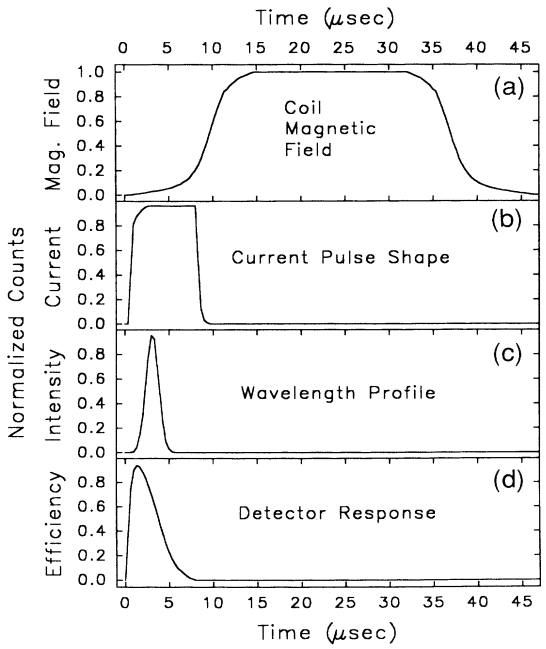

FIG. 9. Normalized profiles of the four factors that give the observed count distributions. (a) The spatial distribution of the magnetic field inside the pulse coil position is converted to time by $x=vt$. (b) The shape for the current pulse applied to the coil. (c) The wavelength spectrum of the incident neutrons; the wavelength shift is converted to a time shift by $\Delta\lambda/\lambda=\Delta t/t$. (d) The efficiency of the ^{3}He detectors in the direction of the beam. All are given in terms of time, but may be converted to length as the neutron velocity is 1.68 mm/μs ($\lambda=2.349$ Å).

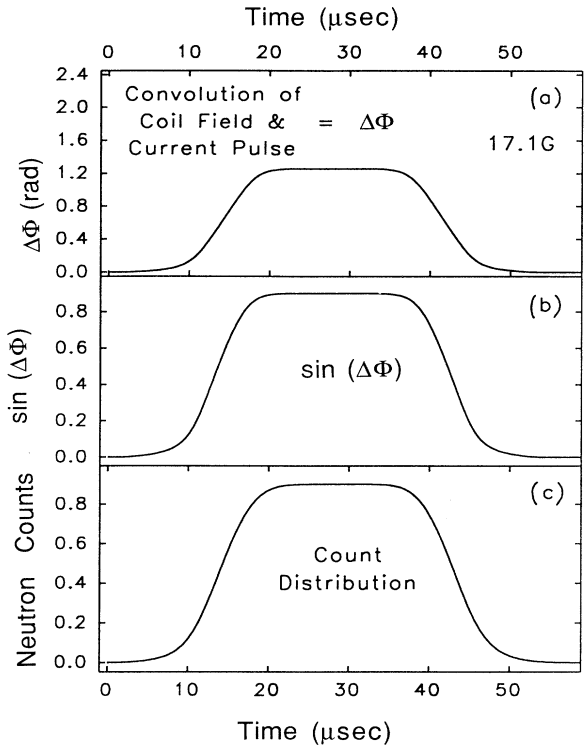

FIG. 10. Derivation of the expected intensity for the scalar AB effect for a pulsed field of 17.1 G. The convolution of Figs. 9(a) and 9(b) gives (a) the profile of the phase shift (magnitude found from a fit to Fig. 8). The counts achieved are then (b) the sine of this phase distribution. This profile is then further convoluted with Figs. 9(c) and 9(d) giving (c) the observed count distribution.

typical settings of bias and pulse amplitudes, is shown in Fig. 6.

Figure 7 displays the count profile of the "down" (against the direction of neutron motion) pulse over the range of pulse coil fields. At the large currents required for the 31.4-G pulse, Joule heating becomes significant in reducing the contrast of the interferometer and as a consequence the count profile is diminished.

Since all the neutron counts, for the increasing pulse coil currents (forward and reverse) were accumulated cyclically in a multiscalar mode as described earlier, it was possible to compare the neutrons that traversed the solenoid for zero current with those that were within the uniform field of the solenoid for the entire duration of the current pulse (thus experiencing an AB phase shift). The number of counts detected is given by Eq. (15) and so the difference in counts in the C_3 detector between positive and negative polarity pulses is

$$N_3(-)-N_3(+)=2N_1b_3\sin(\Delta\phi_{\rm AB}) . \quad (16)$$

This displays the expected sinusoidal profile, as shown in Fig. 8, in clear agreement with the AB prediction.

D. Data analysis

We may consider the magnetic field of the pulse coil, responsible for the phase shift, to be of the form

$$B(x,t)=B_0f(x)g(t) , \quad (17)$$

where $g(t)$ defines the actual current pulse shape and $f(x)$, the field distribution inside the coil, shown normalized to unity in Figs. 9(a) and 9(b), respectively. The phase shift experienced by a neutron starting at x_0, relative to the coil's center at time $t=0$ is then

$$\Delta\phi(x_0,v)=\frac{\mu B_0}{\hbar}\int_{-\infty}^{\infty}f(x_0+vt)g(t)dt , \quad (18)$$

where v is the velocity of the neutron and x_0+vt its distance along the path through the interferometer.

Thus the convolution of g and f defines the profile of the phase shift shown in Fig. 10(a) for a pulsed field of 17.1 G. The magnitude of the expected effect is found by fitting a sinusoidal scaling factor to the data of Fig. 8. The intensity in detector C_3 for a given set of neutrons having initial position x_0 and velocity v is then of the form

$$I(x_0,v)=a+b\sin\Delta\phi(x_0,v) , \quad (19)$$

equivalent to Eq. (15). This distribution is shown in Fig. 10(b) for a field pulse of 17.1 G. The neutrons in the beam, however, have a range of velocities [Fig. 9(c)], and so will cover the distance from the coil center to the detectors in the different times. As well, there is a spatial detection efficiency profile [Fig. 9(d)], along the beam line, through the detector. Convoluting $I(x_0,v)$ with these two distributions has a further smearing effect on

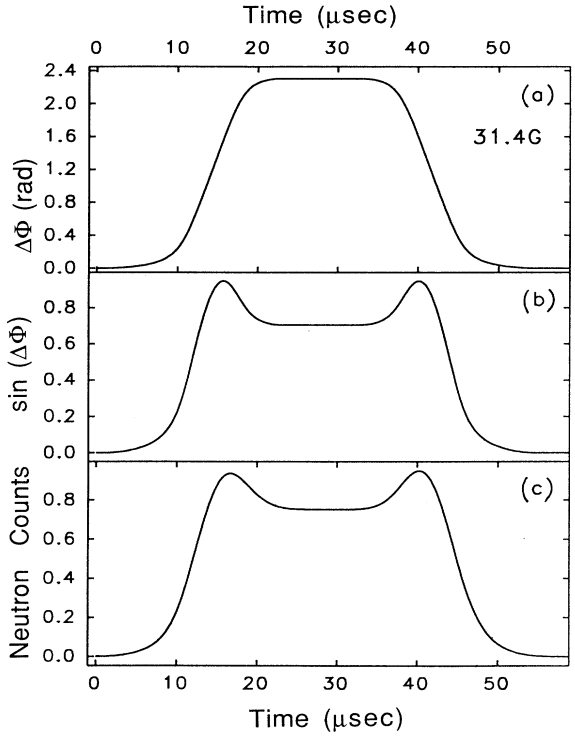

FIG. 11. Derivation of the expected intensity for the scalar AB effect for a pulsed field of 31.4 G. The three panels (a), (b), and (c) have the same meaning as those in Fig. 10.

the observed count profile as shown in Fig. 10(c). The distributions are plotted versus time, rather than position x_0, by using $x_0 = vt$. Equivalent distributions for a pulsed field of 31.4 G are shown in Fig. 11. An example of such a calculation is shown as the fit to the data for a 128-μs scan in Fig. 6. It is seen to be in excellent agreement with the data.

III. CONCLUSIONS

The results reported in this paper clearly confirm the idea put forward in the 1959 Aharonov and Bohm paper [1]. In essence, that paper drew attention to the fact that potentials, even when they were spatially uniform and produced no force, could change the quantum-mechanical motion of the particles in the system. This is a purely quantum-mechanical result, having no counterpart in classical physics. The original Aharonov-Bohm predictions were made for charged particles moving in electromagnetic scalar and vector potentials. The vector-potential predictions have been well confirmed [1–3]. The scalar predictions, difficult to confirm in electrical systems, were shown to have analogs by Zeilinger [17] and Anandan [18,19] for spinning particles. The results agree qualitatively and quantitatively with the quantum predictions for the analog system, comprising thermal neutrons.

In this paper we have reviewed in detail our neutron-interferometric observation of the scalar AB phase shift. Though the most direct demonstration of the scalar AB effect with neutrons would be to use neutrons polarized so their spin was polarized in the same direction as the applied magnetic field, in this experiment an unpolarized beam of neutrons was used. This fact has led to some confusion [21]. Each neutron in an unpolarized beam is, of course, 100% polarized in some direction. However, a neutron in a magnetic field **B** has two eigenstates $\sigma = +1$ and $\sigma = -1$, with respect to the z axis of quantization (along **B**). In this experiment **B** is spatially uniform, but time dependent. Thus, the magnetic field exerts no force on the neutron such that the momentum $\mathbf{p} = m\mathbf{v}$ is a constant of the motion. Nevertheless, the neutron experiences a torque $\boldsymbol{\mu} \times \mathbf{B}$, and therefore precesses about **B** with Larmor frequency $\omega_L = \gamma B$ ($\gamma = 2\mu_n/\hbar$), such that its wave function is

$$\Psi(x,t) = [\cos(\theta/2) e^{-i\omega_L t/2} |\alpha\rangle + i \sin(\theta/2) e^{+i\omega_L t/2} |\beta\rangle] e^{ip_0 x/\hbar - iE_0 t/\hbar}, \quad (20)$$

where θ is the polar angle of the neutron-spin angular-momentum vector **S** with respect to **z**, $|\alpha\rangle$ is the spin-up eigenstate, $|\beta\rangle$ is the spin-down eigenstate, and E_0 is the initial (fixed) kinetic energy of the neutron. It is important to realize that the Larmor precession frequency ω_L is independent of the polar angle θ. Equation (20) shows us that the phase shift for the spin-up state for a magnetic-field pulse of duration Δt is $\Delta\Phi_\uparrow = -\phi_L/2 = -\omega_L \Delta t/2$, and for the spin-down state the phase shift is $\Delta\phi_\downarrow = +\phi_L/2 = +\omega_L \Delta t/2$. The phase shift is $\frac{1}{2}$ the precession angle, a fact which has led to the demonstration of the sign reversal of a Fermion wave function during 2π precession in earlier neutron-interferometry experiments. [24–26]. The fundamental difference between the present experiment and those earlier experiments is that here the magnetic field is spatially uniform, but time dependent. Consequently, in this experiment the magnetic field exerts no force on the neutron, but there still is a phase shift. This is precisely in the spirit of all topological AB-effect experiments. The fact that the phase shift is related to precession is interesting, but for this experiment it is essentially irrelevant.

In the earlier experiments, neutrons on one leg of the interferometer were allowed to pass through a region of magnetic field [24–26]. The neutron thus experiences a force upon entering (and leaving) the magnetic field. The spin-up neutron wave packet is speeded up (slowed down), and the spin-down wave packet is slowed down (speeded up) upon entering (leaving) the region of magnetic field.

It remains an experimental challenge in both neutron and electron AB-effect experiments, and in the neutron AC-effect experiment, to directly verify that the particle velocity is in fact unchanged by the potentials.

ACKNOWLEDGMENTS

This work was supported by the Australian Research Grants Scheme and the U.S. National Science Foundation (Grant No. NSF-PHY-9024608).

[1] Y. Aharonov and D. Bohm, Phys. Rev. **115**, 485 (1959).
[2] For an exhaustive review, see the monograph by M. Peshkin and A. Tonomura, *The Aharonov-Bohm Effect,* Lecture Notes in Physics Vol. 3450 (Springer-Verlag, Berlin, 1989).
[3] R. G. Chambers, Phys. Rev. Lett. **5**, 3 (1960).
[4] G. Möllenstedt and W. Bayh, Physica B **18**, 299 (1962).
[5] A. Tonomura, T. Matsuda, R. Suzuki, A. Fukuhara, N. Osakabe, H. Umezaki, J. Endo, K. Shinagawa, Y. Sugita, and H. Fujiwara, Phys. Rev. Lett. **48**, 1443 (1982); A. Tonomura, Rev. Mod. Phys. **59**, 639 (1987).
[6] W. H. Furry and N. F. Ramsey, Phys. Rev. **118**, 623 (1960).
[7] S. Olariu and I. I. Popescu, Rev. Mod. Phys. **57**, 339 (1985).
[8] G. Mateucci and G. Pozzi, Phys. Rev. Lett. **54**, 2469 (1985).
[9] J. Baumann, J. Kalus, R. Gähler, W. Mampe, and B. Alefeld, Physica B **151**, 130 (1988).
[10] D. M. Greenberger, D. K. Atwood, J. Arthur, C. G. Shull, and M. Schlenker, Phys. Rev. Lett. **47**, 751 (1981).
[11] Y. Aharonov and A. Casher, Phys. Rev. Lett. **53**, 319 (1984).
[12] A. G. Klein, Physica B **137**, 230 (1986).
[13] J. Anandan, Phys. Rev. Lett. **48**, 1660 (1982).
[14] A. Cimmino, G. I. Opat, A. G. Klein, H. Kaiser, S. A.

Werner, M. Arif, and R. Clothier, Phys. Rev. Lett. **63**, 380 (1989).

[15] H. Kaiser, S. A. Werner, R. Clothier, M. Arif, A. G. Klein, G. I. Opat, and A. Cimmino, in *Atomic Physics 12,* edited by Jens C. Zorn and Robert R. Lewis, AIP Conf. Proc. No. 233 (AIP, New York, 1991), pp. 247–268.

[16] A. S. Goldhaber, Phys. Rev. Lett. **62**, 482 (1989).

[17] A. Zeilinger, in *Fundamental Aspects of Quantum Theory,* Vol. 144 of *NATO ASI Series B: Physics,* edited by V. Sorini and A. Frigerio (Plenum, New York, 1985).

[18] J. Anandan, Phys. Lett. A **138**, 347 (1989); **152**, 504 (1991).

[19] J. Anandan, in *Proceedings of the 3rd International Symposium on the Foundations of Quantum Mechanics,* Tokyo, 1989 (Physical Society of Japan, Tokyo, 1990), pp. 98–106.

[20] B. E. Allman, A. Cimmino, A. G. Klein, G. I. Opat, H. Kaiser, and S. A. Werner, Phys. Rev. Lett. **68**, 2409 (1992).

[21] M. Peshkin, Phys. Rev. Lett. **69**, 2017 (1992).

[22] R. Clothier, H. Kaiser, S. A. Werner, H. Rauch, and H. Wölwitsch, Phys. Rev. A **44**, 5357 (1991); S. A. Werner, R. Clothier, H. Kaiser, H. Rauch, and H. Wölwitsch, Phys. Rev. Lett. **67**, 683 (1991).

[23] S. A. Werner and A. G. Klein, in *Methods of Experimental Physics,* edited by K. Skold and D. L. Price (Academic, New York, 1986), Vol. 23, pp. 259–337.

[24] S. A. Werner, R. Colella, A. W. Overhauser, and C. F. Eagen, Phys. Rev. Lett. **35**, 1053 (1975).

[25] H. Rauch, A. Zeilinger, G. Badurek, A. Wilfing, W. Bauspiess, and U. Bonse, Phys. Lett. **54A**, 425 (1975).

[26] A. G. Klein and G. I. Opat, Phys. Rev. D **11**, 523 (1975); Phys. Rev. Lett. **37**, 238 (1976).

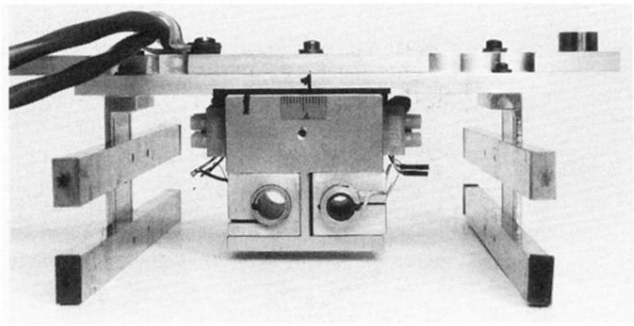

FIG. 5. Photograph of the coil assembly positioned so as to encompass the two arms of the interferometer. The smaller solenoid (right) is the pulsed coil. The quadrupole of bar magnets providing the environment field that establishes the direction for quantization for the neutron spins are seen to the sides.